
جامعة الملك عبدالله
للعلوم والتقنية
King Abdullah University of
Science and Technology

Half-metallic perovskite superlattices with colossal thermoelectric figure of merit

Item Type	Article
Authors	Upadhyay Kahaly, M.; Ozdogan, K.; Schwingenschlögl, Udo
Citation	Kahaly MU, Ozdogan K, Schwingenschlögl U (2013) Half-metallic perovskite superlattices with colossal thermoelectric figure of merit. J Mater Chem A 1: 8406. doi:10.1039/c3ta11346a.
Eprint version	Publisher's Version/PDF
DOI	10.1039/c3ta11346a
Publisher	Royal Society of Chemistry (RSC)
Journal	Journal of Materials Chemistry A
Rights	Archived with thanks to Journal of Materials Chemistry A
Download date	25/02/2022 14:36:01
Link to Item	http://hdl.handle.net/10754/315758

Journal of Materials Chemistry A

RSC Publishing

PAPER

View Article Online
View Journal | View Issue

Published on 09 May 2013. Downloaded by King Abdullah Univ of Science and Technology on 19/03/2014 13:20:08.

Cite this: J. Mater. Chem. A, 2013, 1, 8406

Half-metallic perovskite superlattices with colossal thermoelectric figure of merit

M. Upadhyay Kahaly,[a] K. Ozdogan[ab] and U. Schwingenschlögl*[a]

Received 3rd April 2013
Accepted 8th May 2013

DOI: 10.1039/c3ta11346a

www.rsc.org/MaterialsA

Nowadays heavy experimental efforts are focussed on doped oxide thermoelectrics to increase the thermopower and thermoelectric performance. We propose a high thermoelectric figure of merit for half-metallic $SrTi_{1-x}Co_xO_3$ (x = 0, 0.125, 0.25, 0.375, and 0.5) in a superlattice with $SrTiO_3$, which is stable at high temperatures and in an oxygen environment. The maximal value of Z hardly depends on the doping, while the temperature at which the maximum occurs increases with the Co concentration. The easy tunability from being an insulator to a half-metal under substitutional doping combined with the colossal figure of merit opens up great potential in the emerging field of spin-caloritronics.

I Introduction

As more than half of the energy generated today is lost as waste heat, there are tremendous activities towards techniques for efficient waste heat recovery and heat to electricity conversion.[1] Efficient thermoelectric materials[2–6] have to show a high thermoelectric figure of merit $Z = S^2\sigma/\kappa$, where S, σ, and κ denote the Seebeck coefficient, electrical conductivity, and thermal conductivity, respectively. On the other hand, the power factor $S^2\sigma$ focuses on the behavior of the electrons when thermal conductivity can be ruled out at the two end reservoirs. Interdependence of S, σ, and κ makes it challenging to optimize all these quantities at the same time to obtain an improved Z. A promising strategy for new materials can be the exploitation of the electron spin, as it has been demonstrated that the interdependence of charge and heat currents in thermoelectric materials can be extended by incorporating spin currents into the picture.[7–9] By different directions and/or magnitudes of the spin up and down currents, a net spin polarised current can be achieved, which results in a spin dependent thermoelectric behavior. The generation of a spin current by a temperature gradient would result in a massive reduction of the thermopower loss from Ohmic heat dissipation associated with the electron motion.

Among the materials with enhanced thermoelectric response, such as skutterudites,[10] complex chalcogenides,[11] clathrates,[12] and half-Heusler alloys,[13] oxides[14] are often characterized by a high thermal stability, excellent oxidation resistance, and weak toxicity. However, the room temperature figure of merit is usually low. For example, for $NaCo_2O_4$ (ref. 15) a value of 0.03 is found, for $NaCo_{2-x}Cu_xO_4$ (ref. 16) a value of 0.08, for $Sr_{1-x}La_xTiO_3$ (ref. 17) a value of 0.09, and for Na_xCoO_2 (ref. 18) a value of 0.11 at high Na doping. Good oxide thermoelectrics at room temperature and elevated temperatures as well as understanding of the mechanisms leading to such properties therefore are highly desirable. In particular, the existence of a magnetic state can provide modifications of the transport properties.

Strontium titanate, $SrTiO_3$, is one of the most widely used chemically and compositionally stable perovskite oxides and thus a prototypical candidate for investigation. It finds a range of applications in non-volatile resistive switching memories,[19,20] field effect transistors,[21] and memory storage devices,[22] for instance. Since it has a small lattice mismatch with many other perovskite oxides,[23–25] it can form a wide range of superlattices. In particular, Nb-doped $SrTiO_3$ has been proposed for thermoelectric applications. In the present work we study the consequences of an induced spin polarization in $SrTiO_3$ by Co doping. We will demonstrate the appearance of half-metallicity and a strongly enhanced thermoelectric figure of merit.

II Methods

Our calculations are performed using the full-potential linearized augmented plane wave plus local orbitals method of the WIEN2k code,[26] within the framework of density functional theory. For modelling dopant concentrations from 12.5% to 50% the supercell approach is employed.[27,28] Specifically, we use a $2 \times 2 \times 6$ supercell of the primitive cubic $SrTiO_3$ unit cell with a total of 120 atoms. We dope the supercell only in the lower third in order to achieve a superlattice of alternating layers of pure and doped $SrTiO_3$, compare the schematic presentation of the structure in Fig. 1. A $6 \times 6 \times 2$ Monkhorst–Pack k-mesh is found to be well converged. We take into account the relativistic effects for the core states and use the scalar relativistic approximation for the valence states, *i.e.*, the effect of spin–orbit

[a]KAUST, Physical Science & Engineering, Thuwal, 23955-6900, Kingdom of Saudi Arabia. E-mail: Udo.Schwingenschlogl@kaust.edu.sa; Tel: +966 (0)544700080
[b]Department of Physics, Yildiz Technical University, 34210, Istanbul, Turkey

This journal is © The Royal Society of Chemistry 2013

Published on 09 May 2013. Downloaded by King Abdullah Univ of Science and Technology on 19/03/2014 13:20:08.

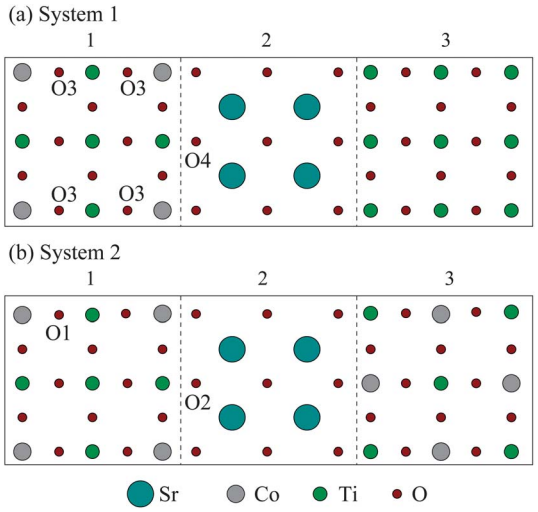


Fig. 1 Schematic representation of the structure, showing atomic layers along the cubic (100) axis. For pristine $SrTiO_3$ this would be alternating layers of TiO_2 and SrO. In systems 1 and 2, respectively, Ti dopings of $x = 0.125$ and $x = 0.5$ were applied.

coupling is not taken into account. The exchange-correlation contribution to the electron–electron interaction is modeled in the generalized gradient approximation.

For the wave function expansion inside the atomic spheres a cutoff of $\ell_{max} = 12$ is used, together with a plane-wave cutoff of $R_{mt}K_{max} = 6$ with $G_{max} = 24$. Our basis set consists of the Sr 4s, 5s, 4p, Ti 4s, 3p, 3d, Co 4s, 3p, 3d, and O 2s, 2p states. All energetically lower states are treated as semi-core and core states. The muffin-tin sphere radii are set to 2.50 a_B for Sr, 1.94 a_B for Ti, 1.8 a_B for Co, and 1.60 a_B for O. All parameters of the calculations have been checked carefully for convergence to obtain the correct results. In order to capture the effects of the structural relaxation on the local chemical bonding and physical properties, the atomic forces in the supercell are converged down to less than 1 mRy a_B^{-1}. For minimizing the Co–Co interaction, we chose distances between the dopant atoms of at least 5.5 Å, using the experimental lattice constant of $SrTiO_3$ (3.905 Å).

For determining the Seebeck coefficients we employed the BoltzTraP code,[29] which is interfaced with WIEN2k. BoltzTraP is based on Boltzmann theory and calculates band structure dependent quantities such as the electrical and thermal conductivities within the rigid band approach. Accurate results require a very fine k-mesh of 3024 points.

III Results

To establish the magnetic ground state, we studied a small $1 \times 1 \times 2$ supercell for 12.5% dopant concentration and optimized its structure assuming non-magnetic, ferromagnetic, and antiferromagnetic configurations for the Co atoms at the Ti sites. We found that the ferromagnetic energy was 41 meV lower than the antiferromagnetic energy, which was 27 meV lower than the non-magnetic energy. Assuming that the magnetic coupling of the Co atoms is given by the mean-field Heisenberg model, we can estimate $T_C = 2/3\ (E_{FM} - E_{AFM})/k_B$[30,31] and obtain for 12.5% Co doping a value of 317 K, which is above room temperature. For a higher concentration the magnetic coupling will increase and T_C will rise.

The effects of Co doping on the otherwise insulating density of states (DOS) of $SrTiO_3$ in the ferromagnetic configuration are demonstrated in Fig. 2 and 3. The total DOS, see Fig. 2 for $x = 0.125$, exhibits an insulating majority spin channel along with a sharp minority spin peak near the Fermi energy (E_F), featuring a half-metallic nature. We have checked whether these properties change under consideration of an onsite interaction on the Co d orbitals. For values between 0 and 6 eV the half-metallic nature remains unchanged. A comparison of the electronic structures obtained without onsite interaction and for a value of 4.8 eV is given in Fig. 2. The DOS shape remains essentially the same but all bands shift to a lower energy in a rather rigid manner under inclusion of the onsite interaction.

In Fig. 3 the partial DOSs of the Co dopant, the nearest neighbouring Ti atom, and the two nearest and next nearest neighbouring O atoms are compared for the lowest and highest doping concentrations. Irrespective of the doping, no Sr states show up in the vicinity of E_F, as to be expected. A high number of Co d states appears at E_F, where the majority of the spin states remain insulated with a gap of about 1 eV (varies slightly with the Co concentration) and the minority spin states give rise to metallicity. A minor Co–Ti hybridization is observed for all doping concentrations. On the other hand, the O DOSs are subject to large modifications next to the dopant. We note that the O atom adjacent to Co in the SrO layer shows a higher DOS at E_F than the one in the TiO_2 layer.

Fig. 4 and 5 elaborate on the consequences of the modified electronic states on the transport behavior of the system and the resulting thermoelectric quantities. Because of the different DOS at E_F, the two spin channels are related to different electrochemical potentials for the same temperature gradient across the sample.[32] The asymmetry of the DOS is the main reason for thermopower (or Seebeck voltage) in classical thermoelectrics.[33] Thus, different asymmetries in the two spin channels lead to different Seebeck coefficients and a net spin dependent Seebeck voltage.[34] The spin dependent Seebeck coefficient, $S_{sp} = S_{up} - S_{dn}$ (where S_{up} and S_{dn} are the Seebeck

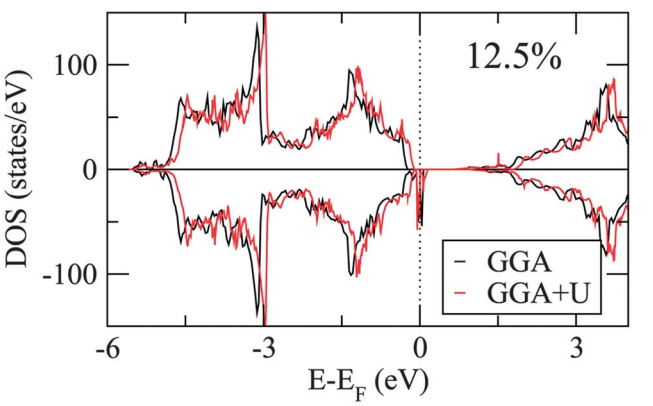


Fig. 2 Total DOS for the $x = 0.125$ superlattice with and without onsite interaction.

Published on 09 May 2013. Downloaded by King Abdullah Univ of Science and Technology on 19/03/2014 13:20:08.

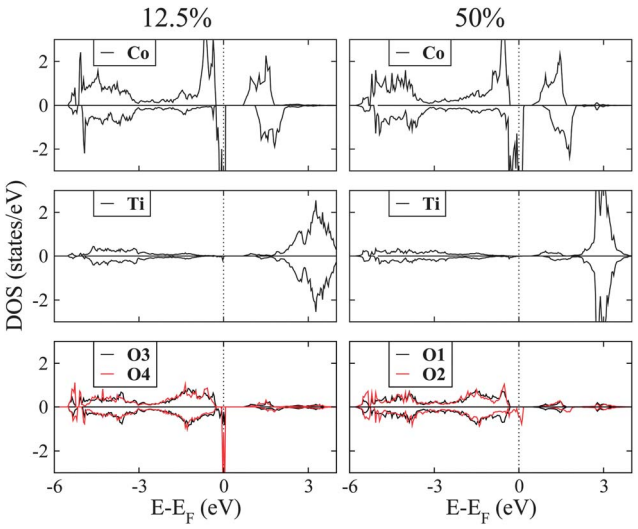


Fig. 3 Partial DOSs for the $x = 0.125$ and $x = 0.5$ superlattices.

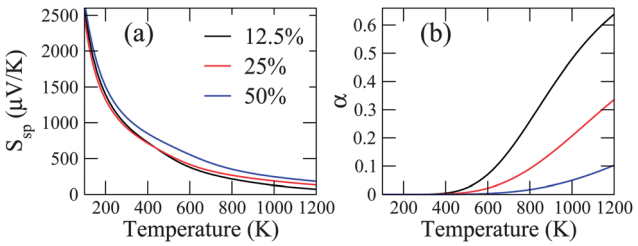


Fig. 4 (a) Spin Seebeck coefficient and (b) spin asymmetry ratio.

coefficients of the up and down spin channels), for different Co concentrations are plotted in Fig. 4(a). A temperature gradient will lead to a spin accumulation proportional to S_{sp}, which is directly measurable with standard lock-in techniques[35] or *via* the spin Hall effect.[36–39] The temperature dependence of S_{sp} is found to be the same for all Co concentrations. At low and room temperature it is high, suggesting an easy generation of spin currents, but decays rapidly with increasing temperature. The scattering spin asymmetry ratio, α, is the ratio of the spin up and down conductivities. Its variation with the temperature is shown in Fig. 4(b). Below room temperature, the majority spin channel is insulating, whereas above approximately 300 K, α grows rapidly. We observe a significant sensitivity to the Co concentration, with an enhanced α for low doping.

The contributions of the two spin channels to the Hall coefficient R_H, the Seebeck coefficient $S = (\sigma_{up}S_{up} + \sigma_{dn}S_{dn})/(\sigma_{up} + \sigma_{dn})$, and the figure of merit Z are addressed in Fig. 5. The shapes of the curves are clearly determined by the metallic minority spin channel. The positive Hall coefficient reflects hole transport, which however declines fast with increasing doping, *i.e.*, injection of additional electrons. Assuming that the relaxation time is direction independent, we find that the Seebeck coefficient increases with the temperature for all Co concentrations. The plateaus in $S(T)$ point at a linear temperature dependence of the thermovoltage above 600 K. While the contributions of the majority spin states to S and the resulting Z remain essentially the same for different dopings, see Fig. 5, changes for the minority spin states show that the two spin channels behave rather independently. Importantly, we find that Co doping always results in a substantial enhancement of the figure of merit, which, however, saturates quickly with the Co concentration. We obtain peak values of 1.50×10^{-3} K^{-1} at 580 K for $SrTi_{0.875}Co_{0.125}O_3$, 1.56×10^{-3} K^{-1} at 630 K for $SrTi_{0.75}Co_{0.25}O_3$, and 1.58×10^{-3} K^{-1} at 780 K for $SrTi_{0.5}Co_{0.5}O_3$.

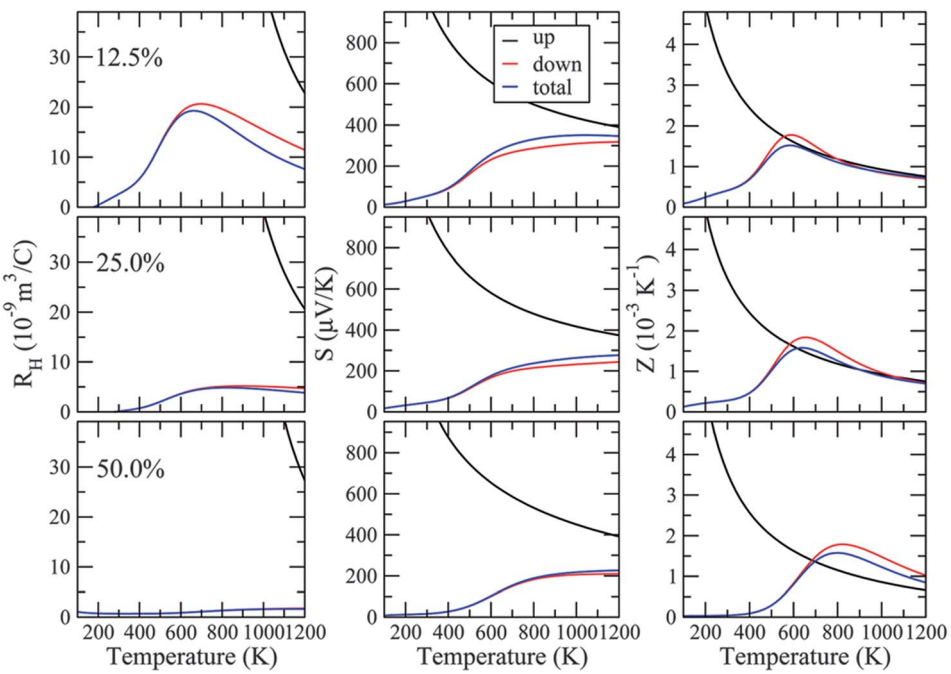


Fig. 5 Spin dependent Hall resistivity, Seebeck coefficient, and figure of merit.

This journal is © The Royal Society of Chemistry 2013

Published on 09 May 2013. Downloaded by King Abdullah Univ of Science and Technology on 19/03/2014 13:20:08.

IV Discussion

Our results demonstrate a strong increase of the thermoelectric figure of merit under Co doping. For example, for Nb-doped $SrTiO_3$ at 300 K a theoretical estimate of 0.3×10^{-3} K^{-1} has been given in ref. 40 for a Nb concentration of 12.5% and an experimental value of 0.12×10^{-3} K^{-1} has been reported for heavy Nb doping.[41] For Co doping of 12.5% we obtain at 300 K a value of $Z = 0.45 \times 10^{-3}$ K^{-1}. This reflects a substantial improvement of the figure of merit in a superlattice of $SrTiO_3$ interfaced with $SrTi_{1-x}Co_xO_3$, driven by the induced spin polarization. The enhancement is even stronger at high temperature. The half-metallicity due to Co doping is mainly carried by the Co d t_{2g} states and prevails under inclusion of an onsite interaction. The majority spin Co d band is fully occupied and located well below E_F, whereas the corresponding minority spin band is partially filled. Assuming that the scattering potential is spin-independent, the minority spin channel thus dominates the conductivity.

Prominently different asymmetries of the majority and minority spin DOSs result in a spin dependent Seebeck voltage, which is proportional to the induced charge accumulation. A high value of the spin Seebeck coefficient irrespective of the Co concentration suggests that the generation of spin currents is not difficult, which makes the superlattice under investigation interesting for the field of spin-caloritronics. We find that the minority spin channel dominates the transport and thus is responsible for the colossal thermoelectric figure of merit over a large doping range. The flat temperature dependence of the Seebeck coefficient (above 600 K) is advantageous from an application point of view. Experimental verification of the theoretical predictions would be desirable.

Acknowledgements

We thank KAUST HPC for providing computational resources. M. Upadhyay Kahaly acknowledges SABIC for financial support and K. Ozdogan thanks the Yildiz Technical University Scientific Research Projects Coordination Department.

References

1 T. M. Tritt, M. A. Subramanian, H. Bottner, T. Caillat, G. Chen, R. Funahashi, X. Ji, M. Kanatzidis, K. Koumoto, G. S. Nolas, J. Poon, A. M. Rao, I. Terasaki, R. Venkatasubramanian and J. Yang, *MRS Bull.*, 2006, **31**, 188.
2 Y. Wang, Y. Sui and W. Su, *J. Appl. Phys.*, 2008, **104**, 093703.
3 J. W. Fergus, *J. Eur. Ceram. Soc.*, 2012, **32**, 525.
4 M. Ito, T. Nagira, D. Furumoto, S. Katsuyama and H. Nagai, *Scr. Mater.*, 2003, **48**, 403.
5 K. Fujita, T. Mochida and K. Nakamura, *Jpn. J. Appl. Phys.*, 2001, **40**, 4644.
6 H. Wang, Y. Pei, A. D. LaLonde and G. J. Snyder, *Adv. Mater.*, 2011, **23**, 1366.
7 G. E. W. Bauer, E. Saitoh and B. J. van Wees, *Nat. Mater.*, 2012, **11**, 391.
8 M. Czerner, M. Bachmann and C. Heiliger, *Phys. Rev. B: Condens. Matter Mater. Phys.*, 2011, **83**, 132405.
9 J. Flipse, F. L. Bakker, A. Slachter, F. K. Dejene and B. J. van Wees, *Nat. Nanotechnol.*, 2012, **7**, 166.
10 B. C. Sales, D. Mandrus and R. K. Williams, *Science*, 1996, **272**, 1325.
11 D.-Y. Chung, T. Hogan, P. Brazis, M. Rocci-Lane, C. Kannewurf, M. Bastea, C. Uher and M. G. Kanatzidis, *Science*, 2000, **287**, 1024.
12 R. T. Littleton, T. M. Tritt, J. W. Kolis and D. R. Ketchum, *Phys. Rev. B: Condens. Matter*, 1999, **60**, 13453.
13 C. Yu, T. Zhu, R. Shi, Y. Zhang, X. Zhao and J. He, *Acta Mater.*, 2009, **57**, 2757.
14 I. Terasaki, Y. Sasago and K. Uchinokura, *Phys. Rev. B: Condens. Matter*, 1997, **56**, R12685.
15 K. Takahata, Y. Iguchi, D. Tanaka, T. Itoh and I. Terasaki, *Phys. Rev. B: Condens. Matter*, 2000, **61**, 12551.
16 I. Terasaki, Y. Ishii, D. Tanaka, K. Takahata and Y. Iguchi, *Jpn. J. Appl. Phys.*, 2001, **40**, 65.
17 T. Okuda, K. Nakanishi, S. Miyasaka and Y. Tokura, *Phys. Rev. B: Condens. Matter*, 2001, **63**, 113104.
18 M. Lee, L. Viciu, L. Li, Y. Wang, M. L. Foo, S. Watauchi, R. A. Pascal Jr, R. J. Cava and N. P. Ong, *Nat. Mater.*, 2006, **5**, 537–540.
19 K. Szot, W. Speier, G. Bihlmayer and R. Waser, *Nat. Mater.*, 2006, **5**, 312.
20 T. Menke, R. Dittmann, P. Meuffels, K. Szot and R. Waser, *J. Appl. Phys.*, 2009, **106**, 114507.
21 T. Sato, K. Shibuya, T. Ohniski, K. Nishio and M. Lippmaa, *J. Appl. Phys.*, 2007, **46**, L515.
22 M. Copel, P. R. Duncomber, D. A. Neumayer, T. M. Shaw and R. M. Tromp, *Appl. Phys. Lett.*, 1997, **70**, 3227.
23 M. Kubo, Y. Oumi, R. Miura, A. Stirling and A. Miyamoto, *Phys. Rev. B: Condens. Matter*, 1997, **56**, 13535.
24 J. Javier and G. Philippe, *Nature*, 2003, **422**, 506.
25 B. H. Lu, S. Y. Dai, Z. H. Chen, L. Yan, Y. L. Zhou and G. Z. Yang, *Chin. Sci. Bull.*, 2003, **48**, 1328.
26 P. Blaha, K. Schwarz, G. Madsen, D. Kvasicka, and J. Luitz, *WIEN2k, An Augmented Plane Wave + Local Orbitals Program for Calculating Crystal Properties*, Technical University of Vienna, Vienna, 2001.
27 U. Schwingenschlögl and C. Schuster, *Europhys. Lett.*, 2009, **86**, 27005.
28 U. Schwingenschlögl and C. Schuster, *Phys. Rev. Lett.*, 2009, **102**, 227002.
29 G. K. H. Madsen and D. J. Singh, *Comput. Phys. Commun.*, 2006, **175**, 67.
30 J. Kudrnovský, I. Turek, V. Drchal, F. Máca, P. Weinberger and P. Bruno, *Phys. Rev. B: Condens. Matter Mater. Phys.*, 2004, **69**, 115208.
31 F. Máca, J. Kudrnovský, V. Drchal and G. Bouzerar, *Appl. Phys. Lett.*, 2008, **92**, 212503.
32 O. Tsyplyatyev, O. Kashuba and V. I. Falko, *Phys. Rev. B: Condens. Matter Mater. Phys.*, 2006, **74**, 132403.
33 R. Zhang, C. Wang, J. Li, J. Zhang, M. Zhao, J. Liu, P. Zheng, Y. Zhang and L. Mei, *Solid State Sci.*, 2010, **12**, 1168.

Published on 09 May 2013. Downloaded by King Abdullah Univ of Science and Technology on 19/03/2014 13:20:08.

34 K. Uchida, S. Takahashi, K. Harii, J. Ieda, W. Koshibae, K. Ando, S. Maekawa and E. Saitoh, *Nature*, 2008, **455**, 778.
35 F. K. Dejene, J. Flipse and B. J. van Wees, *Phys. Rev. B: Condens. Matter Mater. Phys.*, 2012, **86**, 024436.
36 S. Takahashi and S. Maekawa, *Phys. Rev. Lett.*, 2002, **88**, 116601.
37 Y. K. Kato, R. C. Myers, A. C. Gossard and D. D. Awschalom, *Science*, 2004, **306**, 1910–1913.
38 S. O. Valenzuela and M. Tinkham, *Nature*, 2006, **442**, 176–179.
39 T. Seki, Y. Hasegawa, S. Mitani, S. Takahashi, H. Imamura, S. Maekawa, J. Nitta and K. Takanashi, *Nat. Mater.*, 2008, **7**, 125–129.
40 K. Ozdogan, M. U. Kahaly and U. Schwingenschlögl, *Appl. Phys. Lett.*, 2012, **100**, 193110.
41 S. Ohta, T. Nomuro, H. Ohta and K. Koumoto, *J. Appl. Phys.*, 2007, **97**, 034106.

This journal is © The Royal Society of Chemistry 2013